Three-Dimensional Position Control using Sliding Mode Control for Multi-Input Systems

João Filipe Silva
MP-273: Sliding Mode Control

May 14, 2021

Abstract

This document contains the first computational exercise for the Sliding Mode Control (SMC) class. Based on the content given in the lectures, it was requested to formulate an algorithm capable of representing a underactuated Multirotor Aerial Vehicle (MAV) whose three-Dimensional Position and Velocity were to be controled by an SMC method. The controller was implemented in Matlab scripts[1] and plots were generated to illustrate the errors between the real states and their commanded values.

1 Problem Formulation

Consider an underactuated multicopter, represented in practice by drones or eVTOL aircrafts with fixed rotors (non-vectorable and with constant pitch). These vehicles have cascaded translation and rotation dynamics, in such a way that the translation is affected by the rotation, but not the other way around. Their underactuation characteristic refers to the fact that, albeit having movement in six degrees of freedom (three-dimensional position and attitude), only four independent control efforts (magnitude of the resulting thrust and torque on three axes) are applied. As reported in the literature [1], a simple way to deal with this dynamic characteristic is through a hierarchical control structure, in which the attitude control loop is placed internally to the position control loop. Thus, as long as it is possible in practice to make the rotation dynamics much faster than the translation dynamics, both in a closed loop, it is possible to satisfactorily design the laws of translation and rotation control separately.

In this work, only the translational control law design will be addressed. Initially, consider two Cartesian Coordinate Systems (CCS), as shown in Figure 1. The body CCS $\mathcal{S}_b \triangleq \{B; \vec{x}_b; \vec{y}_b; \vec{z}_b\}$ is attached to the MAV (supposedly rigid) structure, with its origin at the MAV center of mass denoted by B, the $\vec{x}_b$ axis pointing forwards, the $\vec{z}_b$ axis normal to the vehicle's structure and pointing upwards, and the $\vec{y}_b$ axis completing an orthonormal dextrogirous basis of the three-dimensional space. The ground (or global) CSS $\mathcal{S}_g \triangleq \{G; \vec{x}_g; \vec{y}_g; \vec{z}_g\}$ is attached to a known point G on the ground, with the $\vec{z}_b$ axis normal to the surface and pointing upwards, and the remaining axes arbitrarily oriented, while satisfying the assumption that they also constitute orthonormal dextrogirous basis of the three-dimensional space. Figure 1 also illustrates the MAV position vector $\vec{r}^{b/g}$, here represented as the position of $\mathcal{S}_b$ with respect to $\mathcal{S}_g$.

[1] All scripts can be found in: https://github.com/jfilipe33/ExCompMP273

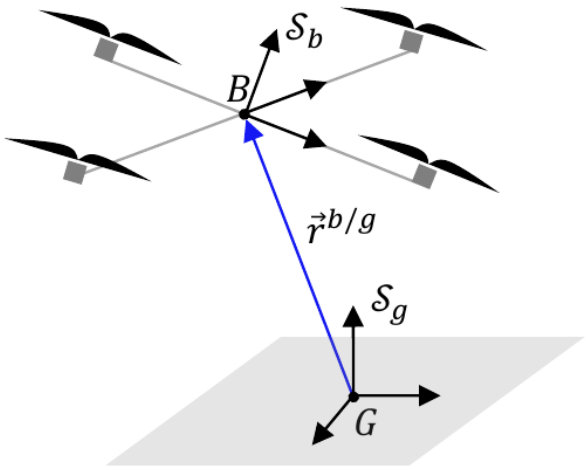

Figure 1: Graphic representation of a underactuated MAV.

Consider that the vehicle has constant mass m and suppose that $\mathcal{S}_g$ represents an itertial reference. Therefore, Newton's Second Law of Motion describes the body movement as:

$$m\frac{^g d^2}{dt}\vec{r}^{b/g} = \vec{f}^{g} + \vec{f}^{c} + \vec{f}^{d}, \tag{1}$$

where $\vec{f}^{g}$, $\vec{f}^{c}$, and $\vec{f}^{d}$ denote the gravity, control and disturbance force vectors, respectively. The superindex g, to the left of the time derivative, indicates that this one is taken with respect to a observer on $\mathcal{S}_g$.

In the translational controller design, instead of using equation (1), which is expressed in Euclidian vectors, it is more convenient to represent the motion in algebric form. Therefore, once each geometric vector in (1) is represented in $\mathcal{S}_g$, we have:

$$m\ddot{\mathbf{r}}_g^{b/g} = \mathbf{f}_g^{g} + \mathbf{f}_g^{c} + \mathbf{f}_g^{d} \tag{2}$$

Finally, assuming $\mathbf{f}_g^{g} \triangleq -mg\mathbf{e}_3$, where g denotes the gravity acceleration magnitude, and $\mathbf{e}_3 \triangleq (0,0,1)$, we obtain:

$$\ddot{\mathbf{r}}_g^{b/g} = -g\mathbf{e}_3 + \frac{1}{m}\mathbf{f}_g^{c} + \frac{1}{m}\mathbf{f}_g^{d} \tag{3}$$

The objective of this exercise is to formulate a Sliding Mode Controller that makes the MAV, whose dynamics are described in (3), follow a desired trajectory even when perturbed by a unknown, but bounded, disturbance signal.

2 Problem Analysis

Let us start by representing the system dynamics, described in equation (3), in State Space regular form for non-linear systems.

$$\begin{aligned} \dot{\mathbf{x}}_1 &= \mathbf{f}_1(\mathbf{x}_1, \mathbf{x}_2) \\ \dot{\mathbf{x}}_2 &= \mathbf{f}_2(\mathbf{x}_1, \mathbf{x}_2) + \mathbf{B}(\mathbf{x}_1, \mathbf{x}_2)(\mathbf{u} + \mathbf{d}) \end{aligned} \tag{4}$$

where $\mathbf{x}_1 \triangleq \mathbf{r}_g^{b/g}$, $\mathbf{x}_2 \triangleq \dot{\mathbf{r}}_g^{b/g}$, $\mathbf{u} \triangleq \mathbf{f}_g^{c}$, and $\mathbf{d} \triangleq \mathbf{f}_g^{d}$.

From (3) and (4), we obtain $\mathbf{B} = \frac{1}{m}$ and:

$$\begin{aligned} \mathbf{f}_1(\mathbf{x}) &= \mathbf{x}_2 \\ \mathbf{f}_2(\mathbf{x}) &= -g\mathbf{e}_3 \end{aligned} \tag{5}$$

The tracking error dynamics can also be modelled in State Space regular form. For that, let us assume $\tilde{\mathbf{x}}_1 \triangleq \mathbf{x}_1 - \bar{\mathbf{r}}_g^{b/g}$ and $\tilde{\mathbf{x}}_2 \triangleq \mathbf{x}_2 - \dot{\bar{\mathbf{r}}}_g^{b/g}$, where $\bar{\mathbf{r}}_g^{b/g}$ represents the desired trajectory. From (3), (4) and the definitions above:

$$\begin{aligned} \dot{\tilde{\mathbf{x}}}_1 &= \tilde{\mathbf{x}}_2 \\ \dot{\tilde{\mathbf{x}}}_2 &= -g\mathbf{e}_3 - \ddot{\bar{\mathbf{r}}}_g^{b/g} + \tfrac{1}{m}(\mathbf{u}+\mathbf{d}) \\ \mathbf{f}_1(\tilde{\mathbf{x}}) &= \tilde{\mathbf{x}}_2 \\ \mathbf{f}_2(\tilde{\mathbf{x}}) &= -g\mathbf{e}_3 - \ddot{\bar{\mathbf{r}}}_g^{b/g} \end{aligned} \tag{6}$$

Let us consider the following assumptions:

- $\left\| \frac{\partial \mathbf{f}_1}{\partial \mathbf{x}_2}(\mathbf{x})\mathbf{B}(\mathbf{x}) \right\| \neq 0, \quad \forall \mathbf{x}$
- $\|\mathbf{d}\| \leq \rho$, with known $\rho > 0$.

The control objective is to design a control law $\mathbf{u} = \nu(\tilde{\mathbf{x}})$ that makes $\tilde{\mathbf{x}} = 0$ a global asymptotically stable equilibrium point of (6). For such a task, lets define the sliding variable as:

$$\sigma(\tilde{\mathbf{x}}) \triangleq \mathbf{C}\tilde{\mathbf{x}}_1 + \mathbf{f}_1(\tilde{\mathbf{x}}) \in \mathbb{R}^3 \tag{7}$$

where $\mathbf{C} \in \mathbb{R}^{3\times 3}$ is a given diagonal positive definite (PD) matrix. Lets also define the corresponding elementary sliding surfaces:

$$\mathcal{S}_i \triangleq \{\tilde{\mathbf{x}} \in \mathbb{R}^n : \sigma_i(\tilde{\mathbf{x}}) = 0\}, \quad i = 1,2,3$$

where $s_i(\mathbf{x})$ denotes the ith component of $\mathbf{s}(\mathbf{x})$.

In particular, the intersection of all the elementary sliding surfaces is called the eventual sliding surface and is denoted by:

$$\mathcal{S} \triangleq \mathcal{S}_1 \cap \mathcal{S}_2 \cap \mathcal{S}_3$$

The sliding motion on $\mathcal{S}$ is called eventual sliding mode; its dynamics are such that $\sigma(\tilde{\mathbf{x}}) = \mathbf{0}$, which from (7) implies

$$\dot{\tilde{\mathbf{x}}}_1 = -\mathbf{C}\tilde{\mathbf{x}}_1 \tag{8}$$

As C is a diagonal and PD by definition, by solving the differential equation in (8), it's possible to see that $(\tilde{\mathbf{x}}_1, \dot{\tilde{\mathbf{x}}}_1) \to \mathbf{0}$ exponentially. As $\dot{\tilde{\mathbf{x}}}_1 \to \mathbf{0}$, then, from (6), $\mathbf{f}_1(\tilde{\mathbf{x}}) \to \mathbf{0}$ exponentially. Consequently, $\tilde{\mathbf{x}}_2 \to \mathbf{0}$ exponentially. Therefore, it's possible to assert that $(\tilde{\mathbf{x}}_1, \tilde{\mathbf{x}}_2) \to \mathbf{0}$ exponentially and $\tilde{\mathbf{x}} = \mathbf{0}$ is an exponentially stable equilibrium point of (6).

For this exercise, the Eventual switching scheme was chosen, in which control law is designed to make $\tilde{\mathbf{x}}$ directly reach the eventual sliding surface $\mathcal{S}$, *i.e.*, it makes $\|\sigma\| \to \mathbf{0}$ in finite time.

The dynamics of σ are obtained by differentiating (7) with respect to time, resulting in:

$$\begin{aligned} \dot{\sigma}(\tilde{\mathbf{x}}) &\triangleq \mathbf{C}\mathbf{f}_1(\tilde{\mathbf{x}}) + \mathbf{f}_2(\tilde{\mathbf{x}}) + \mathbf{B}(\mathbf{u}+\mathbf{d}) \\ \dot{\sigma}(\tilde{\mathbf{x}}) &\triangleq \mathbf{C}\tilde{\mathbf{x}}_2 - g\mathbf{e}_3 - \ddot{\bar{\mathbf{r}}}_g^{b/g} + \tfrac{1}{m}(\mathbf{u}+\mathbf{d}) \end{aligned} \tag{9}$$

For this exercise, lets assume the following given vectors:

$$\mathbf{d}(t) = \begin{bmatrix} 0,3\sin(\pi t/4) \\ 0,4\sin(\pi t/4+\pi/2) \\ 0,5\sin(\pi t/4+\pi) \end{bmatrix} N \qquad \bar{\mathbf{r}}_g^{b/g}(t) = \begin{bmatrix} \sin(\pi t/2) \\ \sin(\pi t/2+\pi/2) \\ t/4 \end{bmatrix} \text{m}$$

To obtain the control law $\mathbf{u}$ that makes $\sigma(\tilde{\mathbf{x}}) = \mathbf{0}$ a global finite-time-stable equilibrium point of (9), first we need to define the maximum disturbance upon the system. When plotting the Phase Portrait of the disturbance vector, figure 2 is obtained. From it, it's possible to see that magnitude of the disturbance vector reaches its maximum value at the points $[-0.3, 0, 0.5]$ and $[0.3, 0, -0.5]$. Said magnitude is obtained by taking the 2-norm of the vector at said points, and it's denoted by $\rho = \|[-0.3;\ 0;\ 0.5]\|_2 = 0.5831$.

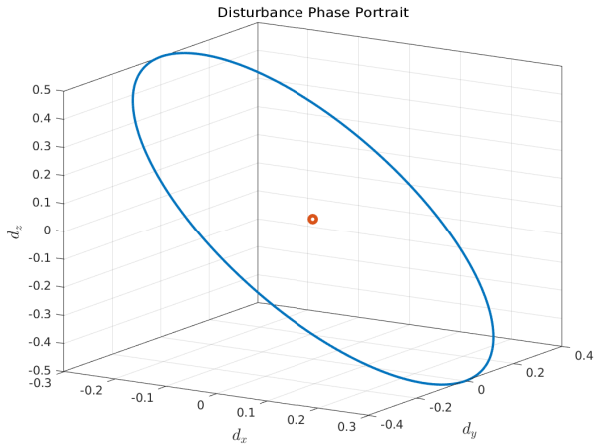

Figure 2: Disturbance Phase Portrait

Now, by defining a control law $\mathbf{u}$ that cancels the known terms in (9), we obtain:

$$\mathbf{u} = -m\left(\mathbf{C}\tilde{\mathbf{x}}_2 - g\mathbf{e}_3 - \ddot{\bar{r}}_g^{b/g} + \kappa\frac{\sigma}{\|\sigma\|}\right) \tag{10}$$

To prove that the control law $\mathbf{u}$ in (10) makes $\sigma(\tilde{\mathbf{x}}) = \mathbf{0}$ a global finite-time-stable equilibrium point of (9), lets consider the following Lyapunov candidate function:

$$V_\sigma(\sigma) = \frac{\sigma^T\sigma}{2} \tag{11}$$

Now, lets calculate the time derivative of (11), and also substitute $\mathbf{u}$ by (10):

$$\begin{aligned} \dot{V}_\sigma(\sigma) &= \sigma^T\dot{\sigma} \\ &= \sigma^T\left(\mathbf{C}\tilde{\mathbf{x}}_2 - g\mathbf{e}_3 - \ddot{\bar{\mathbf{r}}}_g^{b/g} + \frac{1}{m}(\mathbf{u}+\mathbf{d})\right) \\ &= \sigma^T\left(-\kappa\frac{\sigma}{\|\sigma\|} + \frac{1}{m}\mathbf{d}\right) \\ \dot{V}_\sigma(\sigma) &= -\kappa\|\sigma\| + \frac{1}{m}\sigma^T\mathbf{d} \end{aligned} \tag{12}$$

Knowing that $\|AB\| \leq \|A\|\|B\|$ and $\|\sigma^T\| = \|\sigma\|$, equation (12) can be rewritten as:

$$\begin{aligned}
\dot{V}_\sigma(\sigma) &\leq -\kappa\|\sigma\| + \frac{1}{m}\|\sigma^T\mathbf{d}\| \\
&\leq -\kappa\|\sigma\| + \frac{1}{m}\|\sigma^T\|\|\mathbf{d}\| \\
&\leq -\kappa\|\sigma\| + \frac{1}{m}\|\sigma\|\rho \\
\dot{V}_\sigma(\sigma) &\leq -\left(\kappa\ -\frac{1}{m}\rho\right)\|\sigma\|
\end{aligned} \tag{13}$$

From the Bhat-Bernstein Theorem, for $\alpha \in (0,1)$, V radially unbounded e $\dot{V}$ globally negative definite, if there is $\eta > 0$ such that

$$\dot{V}(x) + \eta V(x)^{1-\alpha} \leq 0, \quad \forall x \in \mathbb{R}^{n_x} \tag{14}$$

then $x = 0$ is globally finite-time stable.

From (11), it's possible to see that $\sqrt{V_\sigma(\sigma)} = \frac{||\sigma||}{\sqrt{2}}$. Substituting this in (14), we obtain:

$$\begin{aligned}
&\dot{V}_\sigma(\sigma) + \left(\kappa\ -\frac{1}{m}\rho\right)\|\sigma\| \leq 0 \\
&\dot{V}_\sigma(\sigma) + \left(\kappa\ -\frac{1}{m}\rho\right)\sqrt{2}\sqrt{V_\sigma(\sigma)} \leq 0 \\
&\therefore \eta = \sqrt{2}\left(\kappa\ -\frac{1}{m}\rho\right) \quad and \quad \alpha = 1/2
\end{aligned} \tag{15}$$

As long as η is positive (*i.e.* $\kappa > \rho/m$), $\sigma = \mathbf{0}$ will be a global finite-time-stable equilibrium point of (9), with reaching time bounded by:

$$\begin{aligned}
T(\sigma(0)) &\leq \frac{1}{\eta(1-\alpha)}V_\sigma(\sigma(0))^{1/2} \\
&\leq \frac{2}{\eta}\frac{||\sigma(0)||}{\sqrt{2}} \\
&\leq \frac{\sqrt{2}}{\eta}||\sigma(0)|| \\
T(\sigma(0)) &\leq \frac{||\sigma(0)||}{\kappa\ -\frac{1}{m}\rho}
\end{aligned} \tag{16}$$

3 System Simulation

The MAV used in this simulation will have $m = 1kg$, and we'll consider $g = 9.81m/s^2$ and $\mathbf{C} = \mathbf{I}_3$. For a switching gain of $\kappa = 1$, these are the plots obtained:

Using (16), the reaching time is upper bounded by $T(\sigma(0)) \leq 86.47s$. In figure 3d it is possible to see that the system reaches sliding mode at $T_r \approx 2s$. The 3D position and velocity are tracked with considerable accuracy as seen in figures 3a and 3b, while the control law $\mathbf{u}$ switches with high frequency when sliding mode is reached, as seen in figure 3c. As mentioned before, this exercise employs the eventual sliding mode, which means every component of σ reaches sliding mode simultaneously, which is also illustrated in figure 3d.

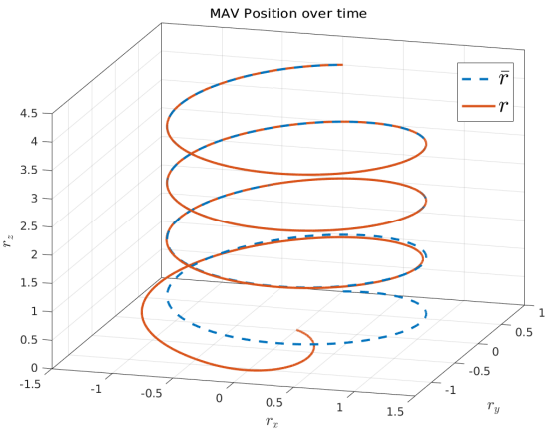

(a) MAV Position over time

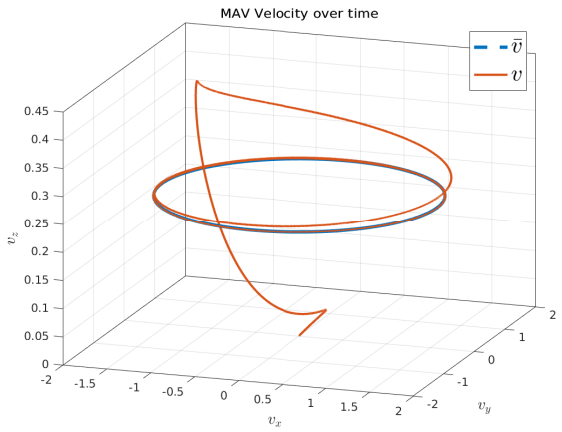

(b) MAV Velocity over time

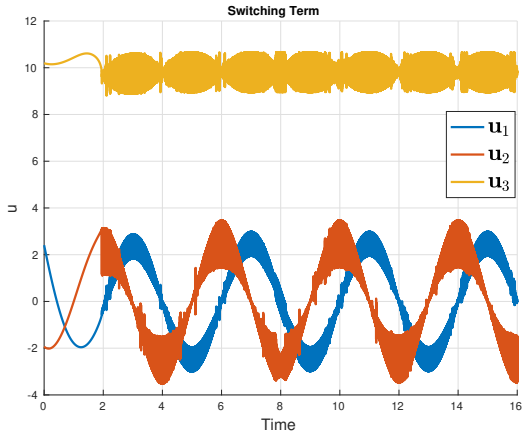

(c) Control Law u

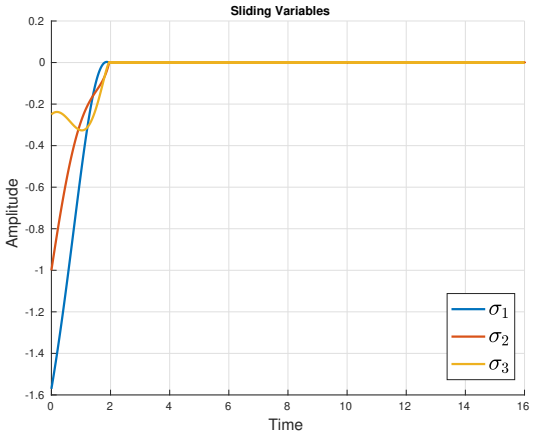

(d) Sliding Variable σ

Figure 3: MAV Position tracking using SMC with Switching Gain $\kappa = 1$.

Now, the switching gain κ was modified to be lower than the disturbance upper limit ρ. Using (16), the reaching time is upper bounded by $T(\sigma(0)) \leq -586.81s$. The negative time is explained by the fact that, for this value of κ, η will be negative and the system will not reach sliding mode. In figure 4d it is possible to see that the system never reaches sliding mode and keeps oscillating. The 3D position is poorly tracked, as the 3D velocity tracking error never reaches zero, as seen in figures 4a and 4b, while the control law $\mathbf{u}$ only switches with high frequency when $\kappa > \|\mathbf{d}\|$, as seen in figure 4c.

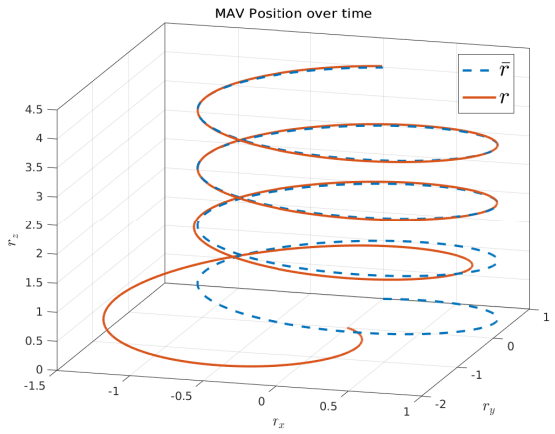

(a) MAV Position over time

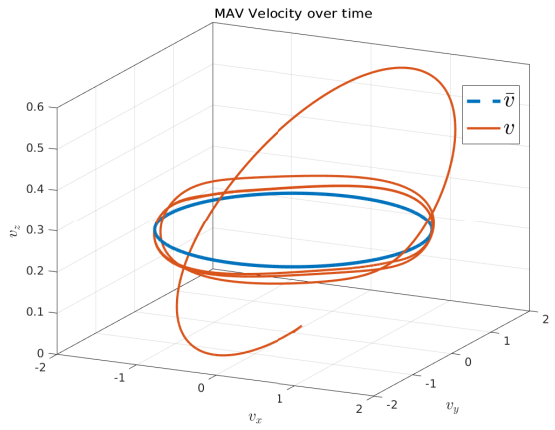

(b) MAV Velocity over time

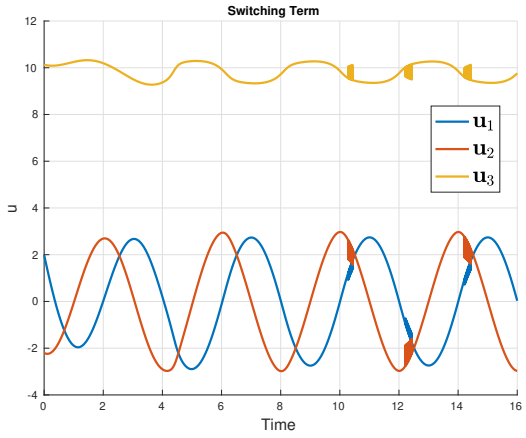

(c) Control Law u

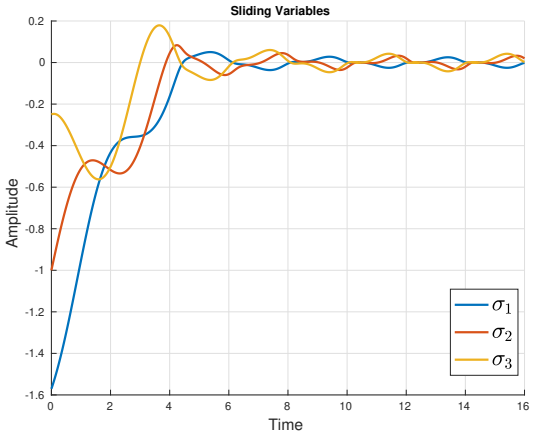

(d) Sliding Variable σ

Figure 4: MAV Position tracking using SMC with Switching Gain $\kappa = 0.5$.

For a last simulation, the switching gain was modified to $\kappa = 3$. The reaching time is upper bounded by $T(\sigma(0)) \leq 9.20s$. In figure 5d it is possible to see that the system reaches sliding mode at $T_r \approx 0.58s$. The 3D position and velocity are tracked with considerable accuracy as seen in figures 5a and 5b, while the control law $\mathbf{u}$ switches with high frequency when sliding mode is reached, as seen in figure 3c. The higher switching gain reduced the reaching time, making the 3D position and velocity values converge to their desired behaviour faster.

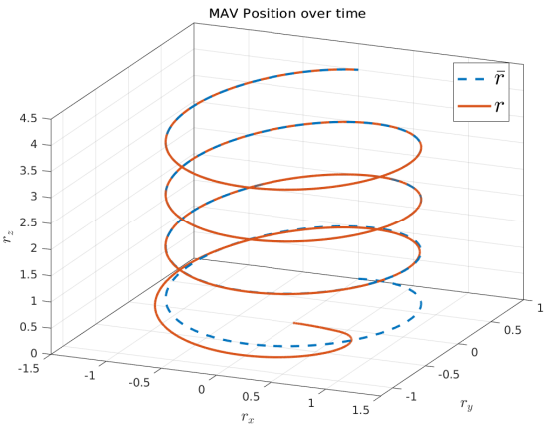

(a) MAV Position over time

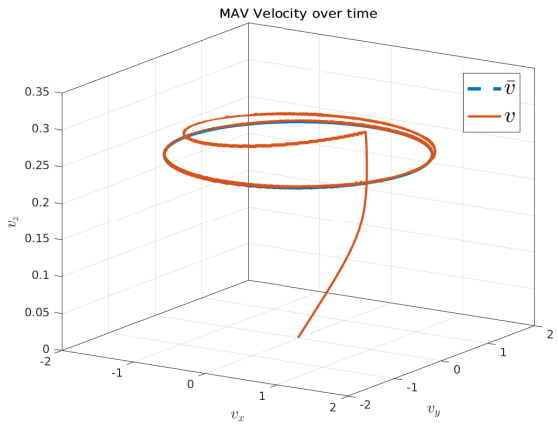

(b) MAV Velocity over time

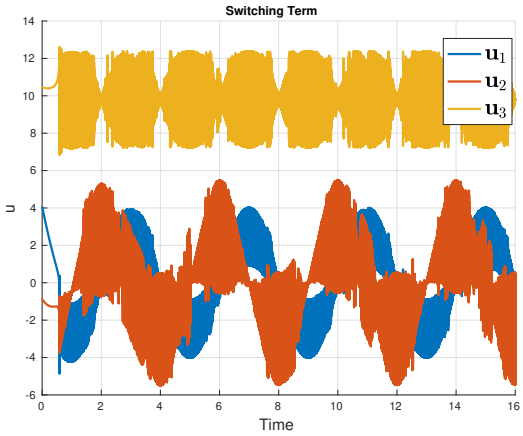

(c) Control Law u

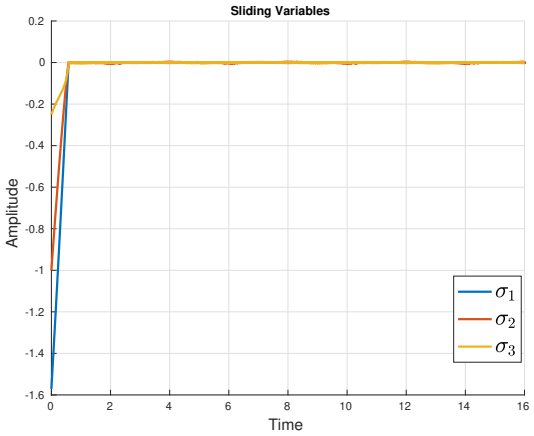

(d) Sliding Variable σ

Figure 5: MAV Position tracking using SMC with Switching Gain $\kappa = 3$.

References

[1] Silva, A. L.; Santos, D. A. Fast Nonsingular Terminal Sliding Mode Flight Control for Multirotor Aerial Vehicles. IEEE Transactions on Aerospace and Electronic Systems, 56(6), 2020.